NANO LETTERS

2007
Vol. 7, No. 1
28−33

λ/4 Resonance of an Optical Monopole Antenna Probed by Single Molecule Fluorescence

Tim H. Taminiau,[†] Robert J. Moerland,[‡] Frans B. Segerink,[‡] Laurens Kuipers,[‡,§] and Niek F. van Hulst*[,†,||]

ICFO—Institut de Ciencies Fotoniques, Mediterranean Technology Park, 08860, Castelldefels (Barcelona), Spain, Applied Optics Group, MESA+ Institute for NanoTechnology, University of Twente, P.O. Box 217, 7500AE Enschede, the Netherlands, and FOM Institute for Atomic and Molecular Physics (AMOLF), Kruislaan 407, 1098 SJ Amsterdam, the Netherlands

Received July 25, 2006; Revised Manuscript Received November 9, 2006

ABSTRACT

We present a resonant optical nanoantenna positioned at the end of a metal-coated glass fiber near-field probe. Antenna resonances, excitation conditions, and field localization are directly probed in the near field by single fluorescent molecules and compared to finite integration technique simulations. It is shown that the antenna is equivalent to its radio frequency analogue, the monopole antenna. For the right antenna length and local excitation conditions, antenna resonances occur that lead to an enhanced localized field near the antenna apex. Direct mapping of this field with single fluorescent molecules reveals a spatial localization of 25 nm, demonstrating the importance of such antennas for nanometer resolution optical microscopy.

Antennas play an essential role as transmitters and receivers in our modern wireless society. The charge movements they support efficiently link propagating electromagnetic fields to localized fields. Radiation from a distant source can be concentrated in a local volume, vice versa a localized excitation can be efficiently coupled into directed radiation. The efficiency of an antenna depends critically on its resonances, as dictated by the operation frequency and by the shape, material, and dimensions of the antenna. Only recently antennas are experimentally explored in the optical domain, where they are crucial to surpass the fundamental diffraction limit. Properly engineered antennas will play a decisive role in the manipulation of light on the nanometer scale, such as control and optimization of emissive systems,[1−3] nanofabrication,[4] optical manipulation and characterization,[5−7] integrated optoelectronic devices, and, as shown in this Letter, subwavelength optical microscopy.[8,9]

So far most research has focused on optical antennas fabricated on planar substrates, restricting their applications. Resonances and coupling effects of such antennas have been investigated thoroughly by linear far-field spectroscopy[10−12] and by exploiting nonlinear responses,[13] such as two-photon luminescence.[14−16] Unfortunately these characterization techniques do not allow a direct local measurement of the electric field. More insight can be obtained using single emitters, such as fluorescent molecules, which are well-defined and direct "point" probes of both local field amplitude and direction.[9,17] To accomplish this, either the emitter or the antenna has to be mounted on a scanning probe. In near-field scanning optical microscopy (NSOM) scattering type probes are used, which exploit the local field enhancement near a sharp tip.[18−20] Such probes could be labeled antennas; however, their infinite size does not support geometrical resonances.[21] Only a few examples of finite-size probe-based antennas have been demonstrated, a gold nanoparticle attached to a glass probe[22−24] and an aluminum bowtie antenna.[2]

All antennas mentioned are illuminated from the far field in a large, at best diffraction limited, focus. The extended illuminated area adds a background contribution to the antenna response. The resulting background problem can be overcome by detection of nonlinear processes[19,25] or by modulation techniques.[20] However, the large illuminated area is unacceptable in fluorescence detection where photobleaching is a primary drawback. Conventional NSOM aperture probes[26] provide a background-free localized excitation volume, but the obtainable field confinement is limited in practice by the low throughput of subwavelength apertures. Frey et al.[27] combined scattering and aperture probes by

* Corresponding author: Niek.vanHulst@ICFO.es.
[†] ICFO—Institut de Ciencies Fotoniques.
[‡] Applied Optics Group, MESA+.
[§] FOM Institute for Atomic and Molecular Physics (AMOLF).
[||] Also at ICREA—Institució Catalana de Recerca i Estudis Avançats, 08015 Barcelona, Spain.

10.1021/nl061726h CCC: $37.00
Published on Web 12/02/2006

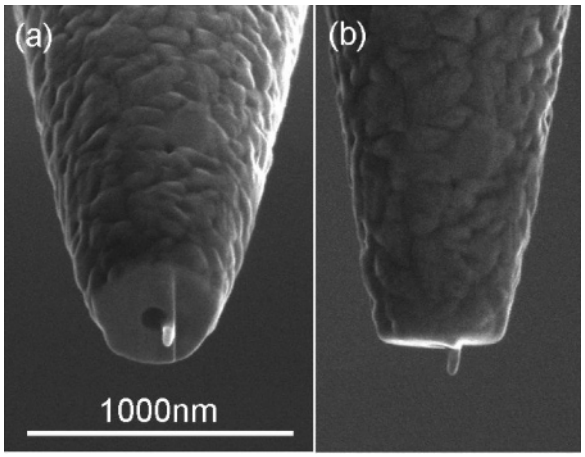

Figure 1. A probe-based nanoantenna (SEM images): (a) viewed from a 52° angle and (b) side view.

placing a sharp metal tip next to a subwavelength aperture. They showed that high optical and topographical resolution can be obtained with reduced background illumination due to the local excitation through the aperture.[28] In principle intensity is sacrificed to reduce the background contribution.

In this Letter we present a probe-based nanoantenna, tuned to resonance by controlling its length. The nanoantenna is excited by placing it in the near field of an aperture fiber probe, providing low background illumination. The antenna response is simulated using the finite integration technique (FIT),[29] giving insight in the antenna excitation conditions and resonance behavior and showing the equivalence of the antenna to the standard monopole antenna. The antenna near field is mapped by single fluorescent molecules in NSOM experiments, thus directly probing the antenna resonances and the field localization down to ~25 nm.

Probe-based antennas are fabricated in a way similar to conventional aperture probes.[26] Sharp glass tips are created by heat-pulling single-mode (633 nm wavelength) glass fibers using a commercial pipet puller (Sutter P2000). Next the probes are coated all-around by evaporation with a few nanometer thick chromium adhesion layer and ~150 nm of aluminum. Aluminum is chosen for its short optical penetration depth. This also implies its optical behavior is relatively close to a perfect electrical conductor (PEC), which favors comparison to the radio antenna analogue. Finally, by focused ion (Ga+) beam (FIB) milling under two different angles, a well-defined elongated antenna (~50 nm width, ~20 nm radius of curvature) is created on a flat end-face next to a circular aperture (100 nm diameter). Figure 1 shows scanning electron microscopy (SEM) images of a resulting probe-based antenna. To investigate the antenna resonances, the antenna length has been controllably varied from 30 to 140 nm. Typical examples are shown in Figure 2. The well-defined antenna probes allow us to investigate their resonant response and compare the experimental behavior directly to FIT simulations.

Three-dimensional FIT simulations are performed using commercial software (CST Microwave Studio).[31] The antenna is modeled as a cylinder with a rounded apex placed next to an aperture (100 nm diameter) in an infinitely large 10 nm thick PEC plate. The plate is illuminated by a plane wave from the top. An overview is shown in Figure 3a. The antenna response is compared to the standard monopole antenna, which consists of antenna element placed on a ground plate that acts like a mirror for the field. Figure 3b shows the concept of a $\lambda/4$ monopole (length equal to a quarter of a wavelength), fed at its base with a current source. Typically, the current source at the base is realized by feeding the monopole via a transmission line at a feed gap or via a coaxial line (Figure 3c). Alternatively, the antenna can be excited from the far field (receiving) (Figure 3d), as is common in optics where transmission lines are still a challenge. Applying a field along the entire antenna is equivalent to inducing a current at the base. Note that the far-field and aperture-illuminated antennas are not loaded by any transmission line (thus there is no feed gap) as the antenna response can be measured by probing the local field instead. On comparison of the field patterns of the response of the actual antenna element in Figure 3, it is clear that the characteristic response is equivalent for the different excitation schemes. This response only depends on the antenna element properties and the quality of the ground plane and not directly on the excitation, which only adds a background field.[30] The aperture is small compared to the wavelength and thus has a relatively minor influence on the efficiency of the ground plate as a reflector. Indeed, simulations for different aperture radii (2−50 nm) do not show any significant change in the characteristic antenna response.

The local field at the aperture drives the antenna. It is anticipated that the antenna is driven by applying a field component along the antenna axis, the *z*-direction (Figure 4a). For an aperture probe it has been shown experimentally[9,17,32−34] and theoretically[35,36] that this component is present at the aperture edges in the direction of the incoming polarization. The antenna is therefore ideally positioned at the edge of the aperture. Parts b and c of Figure 4 show the field intensity evaluated in a plane 10 nm below the antenna apex. For the polarization in the direction of the line through the centers of the aperture and the antenna (Figure 4b), a field component along the antenna axis is present. The antenna is excited, and a highly localized enhanced field forms at the antenna apex. The full width at half-maximum (fwhm) of the intensity pattern is 27 nm for the conditions in Figure 4b. For the perpendicular polarization, no such field is formed and only the 2 orders of magnitude weaker intensity distribution originating from the aperture is found (Figure 4c).

The antenna resonances are determined by the size, shape, and material parameters of the antenna. Figure 5 illustrates the resonances by varying the length for three antennas of different radius and material properties, all at $\lambda = 514$ nm. For a 2 nm radius PEC antenna the imaginary part of the input impedance of the antenna goes to zero for lengths slightly less than uneven multiples of $\lambda/4$ (115 nm, 365 nm); resonance occurs and a strong field is formed at the antenna apex, 90° out of phase with the driving field (see full phase cycle online). The phase lag of a quarter optical cycle is a clear signature of resonant response. The even multiples of

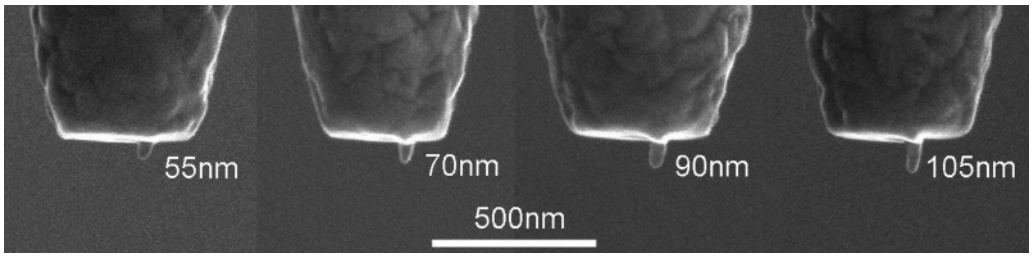

Figure 2. Tuning the antenna length to investigate its resonance. Length: 55 ± 5 nm, 70 ± 5 nm, 90 ± 5 nm, and 105 ± 5 nm (SEM images).

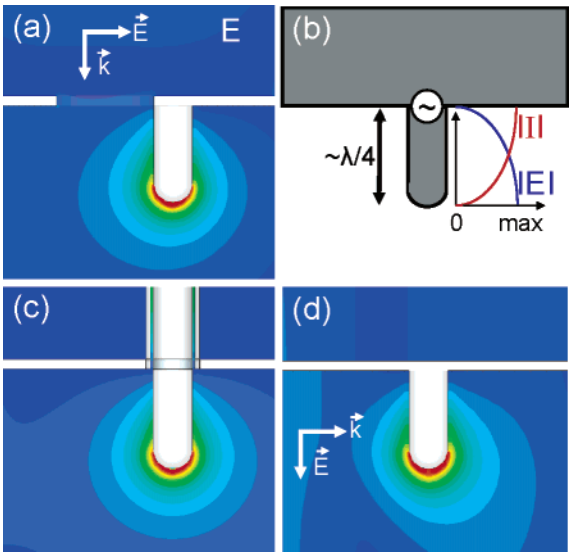

Figure 3. Monopole antennas and excitation configurations. (a) Cross section of the probe-based antenna configuration. (b) Conceptual description of a base-fed $\lambda/4$ monopole antenna and the associated characteristic current $|I|$ and field $|E|$ distributions. (c) Coaxially fed monopole. (d) Far-field illuminated monopole. The instantaneous field of the characteristic antenna response is shown and is equivalent for all the excitation schemes.[30]

$\lambda/4$ in length are antiresonances, modes without net dipole moment,[37,38] resulting in minimum field strength. This behavior is characteristic for a thin wire monopole antenna. To illustrate this, the calculated resonances for a coaxially fed 2 nm PEC monopole antenna (configuration shown in Figure 3c) are also indicated in Figure 5.

Increasing the radius of the antenna shifts the resonance to shorter length (~100 nm) and increases the bandwidth (or peak width) due to the end effect.[39] This is illustrated in Figure 5 for a 20 nm radius PEC antenna. Aluminum is not a PEC at optical frequencies. For $\lambda = 514$ nm, the complex dielectric constant of aluminum is $\epsilon = -31.3 + 8.0i$, as determined by fitting a Drude model to experimental values.[40] For an aluminum antenna the resonance shifts to even shorter length (~70 nm). Although the free space wavelength is kept constant, the wavelength of the standing-wave charge oscillation at resonance along/in the antenna is shortened for both thicker and imperfect metal antennas. Thus, the relatively thick optical (complex dielectric function) antennas have resonances at shorter length than analogous thin radio-wave (PEC) antennas, while retaining characteristic field distributions.[30] Note that the second resonance of the aluminum antenna (at a length equal to $^3/_4\lambda$ of the charge oscillation) coincides with the first antiresonance for a thin PEC antenna (at $\lambda/2$ of the free wave). Again the resonance lengths for equivalent coaxially fed monopoles are marked in the figure. As expected from the previous discussion the resonance lengths for aperture and coaxial fed antennas are in good agreement.

To experimentally verify the properties of the nanoantenna, single fluorescent molecules are used to map the local antenna field. To this end samples consisting of isolated DiI-molecules in a 10−20 nm thick PMMA layer are prepared by spin coating. The single-molecule samples are scanned underneath the antenna probe using a near-field scanning optical microscope with shear-force feedback, as described

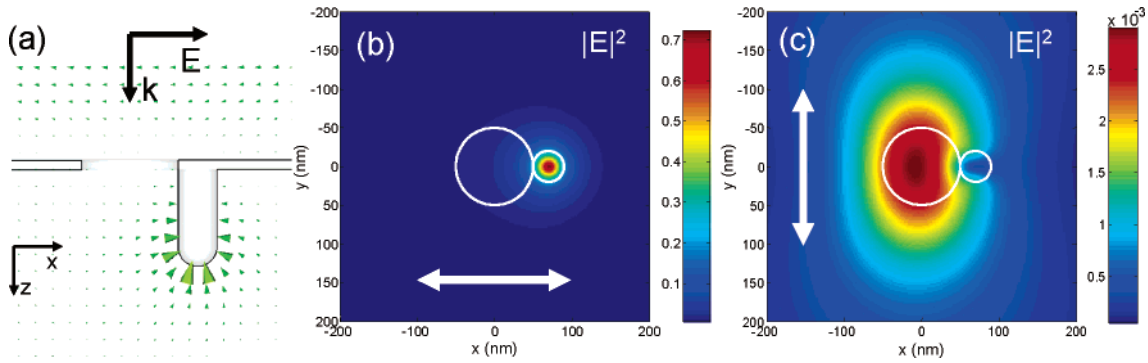

Figure 4. Field localization and polarization-dependent excitation of the antenna (FIT simulations). (a) A cross section of the antenna structure (length of 100 nm, radius 20 nm, PEC, $\lambda = 514$ nm) and the resulting field (instantaneous; full phase cycle available online). (b, c) The time-averaged intensity normalized to the incoming wave intensity is evaluated in a plane 10 nm below the antenna apex for two polarization directions of the incoming plane wave (see arrows): (b) in the direction of the antenna and (c) the direction perpendicular to that. The large circle represents the aperture (radius 50 nm) the small one the antenna (radius 20 nm).

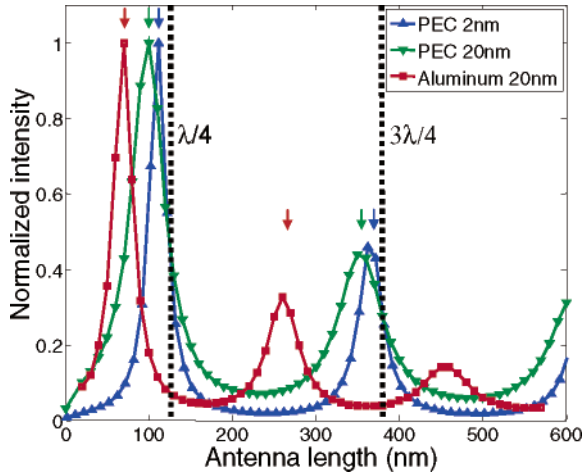

Figure 5. Calculated antenna resonances. The field intensity 5 nm below the antenna apex normalized on the maximum against the antenna length for different antennas: perfect electrical conducting (PEC) radius 2 nm (blue line, upward triangles, maximum = 17.5) and 20 nm (green line, downward triangles, maximum = 0.8), aluminum radius 20 nm (red line, circles, maximum = 0.95). λ = 514 nm. The colored arrows mark the calculated resonance lengths of the corresponding coaxially fed monopoles.

in detail earlier.[41] In order to control the excitation polarization at the probe's end face, the polarization of the laser light (λ = 514 nm, Ar^+ line) is adjusted before being coupled into the probe fiber and characterized after being emitted from the probe. The collected molecular fluorescence is filtered from the exciting laser light, split into two branches by a polarizing beam splitter, and detected by photon counting avalanche photodiodes (APDs). This way the polarization of the fluorescence is monitored and information about the orientation of the molecular emission dipole is obtained.

Panels a−c of Figure 6 show the single molecule fluorescence response for an 80 nm long antenna. For an excitation polarization in the direction of the antenna (Figure 6a) narrow single molecular patterns are found together with several weaker larger spots originating from the background illumination from the aperture. When the polarization direction is rotated by 90° (Figure 6b), only large weak spots are found. With restoration of the polarization (Figure 6c), the original image with narrow patterns is recovered, proving that the effect is purely optical. Indeed, as predicted by simulations, a highly localized field is formed at the antenna apex for the right polarization of the excitation. Figure 6f shows a cross section from a closeup scan of one of the molecules in Figure 6a. A width (fwhm) of 26 ± 5 nm is found for a Gaussian fit, in good agreement with the value found for the simulated intensity pattern. This confirms that the field is highly localized and bound to the antenna dimensions. The narrow field confinement effectively demonstrates the strength of antenna-based high-resolution NSOM.

The color coding in the images gives information on the orientation of the emission dipole of the molecules. Like for conventional aperture probes, the aperture mainly excites molecules with an absorption dipole orientated along the excitation polarization[17] and large molecular features with an emission polarization parallel to the excitation polarization

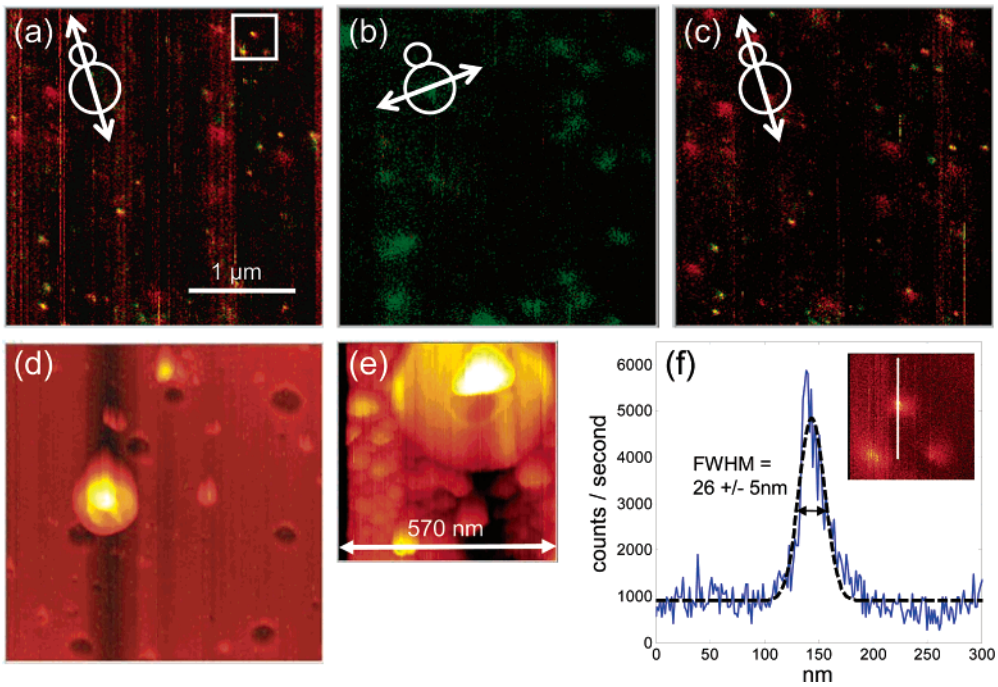

Figure 6. Single molecule NSOM experiments revealing narrow patterns for the right excitation polarization, indicating a highly localized field. Fluorescence (a, b, c, f) and topographical results (d) for an antenna of 80 ± 5 nm length. The incoming polarization is in the direction of the antenna for (a) and (c), perpendicular to that for (b) (see inset: antenna, small circle; aperture, larger circle; polarization, arrow). The color scaling represents the polarization of the collected fluorescence. Red is vertical; green is horizontal.[41] (d) Topography obtained simultaneously with scan (a). (e) Closeup of a topographic antenna feature for a different probe. (f) Cross section of the intensity profile of one of the molecules in (a) and Gaussian fit (black dashed line) showing a width of 26 ± 5 nm.

are found. The antenna field contains local components in all directions (Figure 4a) and can actually excite molecules of various orientations, as can be seen from the variety of emission polarizations found for the different narrow patterns. A full analysis of the molecular orientation and its effect on the patterns is complicated by the observation that the presence of the antenna influences the molecular emission and is therefore not pursued here.

In contrast to our data, Frey et al.[28] reported molecular patterns with dark spots in the center of the patterns for molecules directly on mica, which has been attributed partly to quenching of the fluorescence by the metal tip. We use molecules embedded in a 10−20 nm polymer layer, thick enough to minimize quenching influences. Indeed, in general we do not observe such dark spots and characteristic patterns are shown in the inset of Figure 6f.

The single molecule fluorescence is not correlated to the simultaneously recorded surface topography (Figure 6d), confirming that the narrow optical response is not height induced. Interestingly, topographical responses that provide valuable information on the antenna structure can be observed. Figure 6d shows a large feature caused by the convolution of the probe with a surface particle that is higher than the antenna length. A clearer example, for another probe, is presented in Figure 6e. The antenna, the flat end-face of the probe, and even the aperture can clearly be recognized. The orientation of the antenna with respect to the aperture can directly be determined. The topographic height gives an independent and precise measurement of the antenna length taken in situ during the actual measurement and thus allows continuous monitoring of the antenna length.

To directly probe the influence of antenna resonances, single molecules have been excited by antennas of different length. As a direct comparison of intensities between probes is impossible, the ratio of the intensities of the narrow antenna patterns (fwhm ∼25 nm) and the large aperture features (fwhm >80 nm) is taken as a measure for the antenna efficiency. An average over several of the strongest most clearly resolvable patterns is taken, thus partly averaging out any influences of molecular orientation and position in the polymer matrix on the efficiency ratio. Figure 7a plots the antenna efficiency against the antenna length. Antennas of a length between 70 and 90 nm show a high efficiency (Figure 7c), while shorter (Figure 7b) and longer (Figure 7d) antennas are found to be less efficient. To compare the results with the calculated resonances, the curve of Figure 5 has been divided by the decay of the field intensity with distance for an aperture. Even though each measurement is done with a different probe and the precise molecular orientations and positions are not taken into account, the results are in good agreement with the calculated antenna efficiency curve. Maximum efficiency is found for antenna lengths around 75 nm, indicating a strong field at the antenna apex and thus resonance. This confirms that the $\lambda/4$-resonance length of the optical monopole antenna is shortened compared to that of the analogous radio monopole antenna, as predicted in Figure 5.

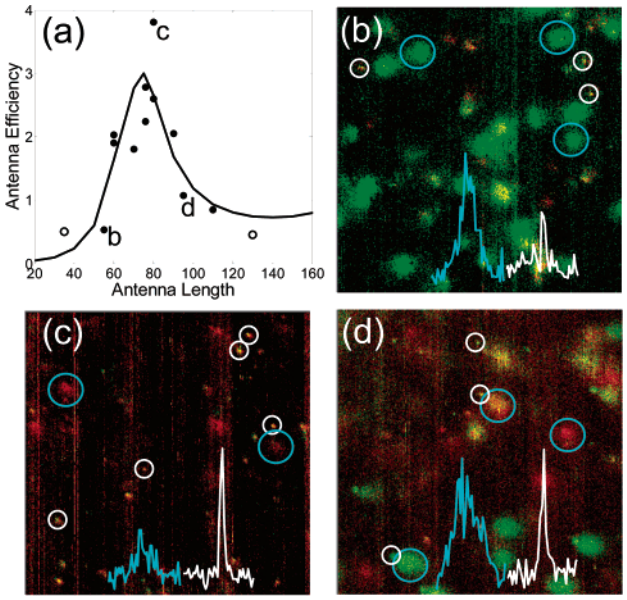

Figure 7. Probing the antenna resonances by varying the antenna length. (a) The antenna efficiency, defined as the intensity ratio of antenna and aperture patterns, against the antenna length. Open circles represent probes for which no narrow antenna patterns are detected; here a maximum intensity has been estimated from the noise level. The solid line is the resonance curve of Figure 5 corrected for the field decay of an aperture (arbitrarily scaled). (b−d) Single molecule fluorescence response for antennas of increasing length: (b) 55 nm, (c) 80 nm, (d) 95 nm. The insets are characteristic cross sections (all 500 nm in length) of the correspondingly marked molecular patterns. The patterns associated with the antenna (fwhm ∼25 nm) are marked with small white circles, those with the aperture field (fwhm >80 nm) with large blue circles. All images are 3 μm × 3 μm.

In conclusion, resonances and field localization of probe-based optical monopole antennas have been directly demonstrated by single fluorescent molecule experiments. Clear polarization-dependent excitation conditions are observed that agree with FIT simulations. By controlling the antenna length, we have revealed a resonant behavior in good agreement with FIT simulations, which show that the finite thickness and material parameters of the optical antennas reduce the effective $\lambda/4$-resonance length compared to analogous radio antennas. The enhanced localized field formed at the antenna apex for the right excitation conditions and resonant antenna length is shown to be confined laterally within 25 nm fwhm, demonstrating the importance of such antennas for nanometer resolution optical microscopy.

Acknowledgment. This work has benefited from support by the Specific Target Research Project (STRP) ASPRINT (NMP-CT-2003-001601) in the sixth Framework Program of the European Community. This work is part of the research program of the Stichting voor Fundamenteel Onderzoek der Materie (FOM), which is financially supported by the Nederlandse Organisatie voor Wetenschappelijk Onderzoek (NWO). Finally we thank Computer Simulation Technology (CST), Darmstadt, Germany, for constructive feedback on the use of Microwave Studio.

Supporting Information Available: Antenna field calculations: full phase cycles and intensity images at resonance for different antennas. This material is available free of charge via the Internet at http://pubs.acs.org.

References

(1) Greffet, J.-J. *Science* **2005**, *308*, 1561.
(2) Farahni, J. N.; Pohl, D. W.; Eisler, H.-J.; Hecht, B. *Phys. Rev. Lett.* **2005**, *95*, 017402.
(3) Gersen, H.; Garcia-Parajo, M. F.; Novotny, L.; Veerman, J. A.; Kuipers, L.; van Hulst, N. F. *Phys. Rev. Lett.* **2001**, *85*, 5312.
(4) Sundaramurthy, A.; Schuck, P. J.; Conley, N. R.; Fromm, D. P.; Kino, G. S.; Moerner, W. E. *Nano Lett.* **2006**, *6*, 355.
(5) Novotny, L.; Bian, R. X.; Xie, X. S. *Phys. Rev. Lett.* **1997**, *79*, 645.
(6) Hartschuh, A.; Sánchez, E. J.; Xie, X. S.; Novotny, L. *Phys. Rev. Lett.* **2003**, *90*, 095503.
(7) Fromm, D. P.; Sundaramurthy, A.; Kinkhabwala, A.; Schuck, P. J.; Kino, G. S.; Moerner, W. E. *J. Chem. Phys.* **2006**, *124*, 061101.
(8) Pohl, D. W.; Denk, W.; Lanz, M. *Appl. Phys. Lett.* **1984**, *44*, 651.
(9) Betzig, E.; Chichester, R. J. *Science* **1993**, *262*, 1422.
(10) Fromm, D. P.; Sundaramurthy, A.; Schuck, J.; Kino, G.; Moerner, W. E. *Nano Lett.* **2004**, *4*, 957.
(11) Crozier, K. B.; Sundaramurthy, A.; Kino, G. S.; Quate, C. F. *J. Appl. Phys.* **2003**, *94*, 4632.
(12) Rechberger, W.; Hohenau, A.; Leitner, A.; Krenn, J. R.; Lamprecht, B.; Aussenegg, F. R. *Opt. Commun.* **2003**, *220*, 137.
(13) Mühlschlegel, P.; Eisler, H.-J.; Martin, O. J. F.; Hecht, B.; Pohl, D. W. *Science* **2005**, *308*, 1607.
(14) Bouhelier, A.; Bachelot, R.; Lerondel, G.; Kostcheev, S.; Royer, P.; Wiederrecht, G. P. *Phys. Rev. Lett.* **2005**, *95*, 267405.
(15) Schuck, P. J.; Fromm, D. P.; Sundaramurthy, A.; Kino, G. S.; Moerner, W. E. *Phys. Rev. Lett.* **2005**, *94*, 017402.
(16) ten Bloemendal, D.; Ghenuche, P.; Quidant, R.; Cormack, I. G.; Loza-Alvarez, P.; Badenes, G. *Plasmonics* **2006**, *1*, 41.
(17) Veerman, J. A.; Garcia-Parajo, M. F.; Kuipers, L.; van Hulst, N. F. *J. Microsc.* **1999**, *194*, 477.
(18) Zenhausern, F.; Martin, Y.; Wickramasinghe, H. K. *Science* **1995**, *269*, 1083.
(19) Sánchez, E. J.; Novotny, L.; Xie, X. S. *Phys. Rev. Lett.* **1999**, *82*, 4014.
(20) Gerton, J. M.; Wade, L. A.; Lessard, G. A.; Ma, Z.; Quake, S. R. *Phys. Rev. Lett.* **2004**, *93*, 180801.
(21) Krug, J. T., II; Sánchez, E. J.; Xie, X. S. *J. Chem. Phys.* **2002**, *116*, 10895.
(22) Kalkbrenner, T.; Håkanson, U.; Schädle, A.; Burger, S.; Henkel, C.; Sandoghdar, V. *Phys. Rev. Lett.* **2005**, *95*, 200801.
(23) Anger, P.; Bharadwaj, P.; Novotny, L. *Phys. Rev. Lett.* **2006**, *96*, 113002.
(24) Kühn, S.; Håkanson, U.; Rogobete, L.; Sandoghdar, V. *Phys. Rev. Lett.* **2006**, *97*, 017402.
(25) Stöckle, R. M.; Suh, Y. D.; Deckert, V.; Zenobi, R. *Chem. Phys. Lett.* **2000**, *318*, 131.
(26) Veerman, J. A.; Otter, A. M.; Kuipers, L.; van Hulst, N. F. *Appl. Phys. Lett.* **1998**, *72*, 3115.
(27) Frey, H. G.; Keilmann, F.; Kriele, A.; Guckenberger, R. *Appl. Phys. Lett.* **2002**, *81*, 5030.
(28) Frey, G. F.; Witt, S.; Felderer, K.; Guckenberger, R. *Phys. Rev. Lett.* **2004**, *93*, 200801.
(29) Weiland, T. *Electron. Commun. AEU* **1977**, *31*, 116.
(30) More field calculations available online as Supporting Information.
(31) CST Microwave Studio 5.1, www.cst.com.
(32) Naber, A.; Molenda, D.; Fischer, U. C.; Maas, H.-J.; Höppener, C.; Lu, N.; Fuchs, H. *Phys. Rev. Lett.* **2002**, *89*, 210801.
(33) Moerland, R. J.; van Hulst, N. F.; Gersen, H.; Kuipers, L. *Opt. Express* **2005**, *13*, 1604.
(34) Molenda, D.; Colas des Francs, G.; Fischer, U. C.; Rau, N.; Naber, A. *Opt. Express* **2005**, *13*, 10688.
(35) Bouwkamp, C. J. *Phillips Res. Rep.* **1950**, *5*, 321. Bouwkamp, C. J. *Phillips Res. Rep.* **1950**, *5*, 401.
(36) Martin, O. J. F.; Paulus, M. *J. Microsc.* **2002**, *205*, 147.
(37) Aizpurua, J.; Bryant, G. W.; Richter, L. J.; García de Abajo, F. J.; Kelley, B. K.; Mallouk, T. *Phys. Rev. B* **2005**, *71*, 235420.
(38) Imura, K.; Nagahara, T.; Okamoto, H. *J. Chem. Phys.* **2005**, *122*, 154701.
(39) Balanis, C. A. *Antenna Theory*: *Analyses and Design*, 3rd ed.; John Wiley: Hoboken, NJ, 2005. ISBN: 0-471-66782-X.
(40) (a) Hass, G.; Waylonis, J. E. *J. Opt. Soc. Am.* **1960**, *50*, 1133. (b) Schultz, L. G.; Tangherlini, F. R. *J. Opt. Soc. Am.* **1954**, *44*, 362. (c) Schultz, L. G. *J. Opt. Soc. Am.* **1954**, *44*, 357.
(41) Ruiter, A. G. T.; Veerman, J. A.; Garcia-Parajo, M. F.; van Hulst, N. F. *J. Phys. Chem. A* **1997**, *101*, 7318.

NL061726H